JMEPEG (2004) 13:710-719
DOI: 10.1361/10599490421349

1059-9495/$19.00

Processing, Deformation, and Failure in Superplastic Aluminum Alloys: Applications of Orientation-Imaging Microscopy

Keiichiro Oh-ishi, John Boydon, and Terry R. McNelley

(Submitted August 23, 2004)

The importance of grain size refinement in enabling superplasticity is reviewed, and the current understanding of grain boundary characteristics is summarized. The application of orientation-imaging microscopy (OIM) methods to the processing response and the deformation and failure modes in superplastic aluminum alloys are illustrated through microtexture analysis and determination of grain boundary characteristics in selected commercial materials. Continuous and discontinuous recrystallization reactions exhibit distinct microtextures and grain boundary characteristics. The application of OIM and microtexture analysis to the evaluation of both deformation and failure mechanisms during superplastic forming is illustrated.

Keywords aluminum, cavity growth, continuous recrystallization, deformation microstructures, deformation processing, deformation textures, discontinuous recrystallization, grain boundaries, grain refinement, recrystallization, superplasticity

1. Introduction: Grain Size and Grain Boundaries in Superplasticity

Highly refined grains and grain boundaries that can sustain sliding without undergoing tensile separation are required to enable superplasticity. Constitutive models for elevated-temperature deformation illustrate the importance of grain size control, but the specific requirements of the grain boundaries in superplasticity are not as well understood. Recently developed orientation-imaging microscopy (OIM) methods may be used to obtain ample data for the characterization of grain boundaries in superplastic aluminum alloys.

For wrought aluminum alloys, grain refinement for superplasticity can be accomplished only by deformation and recrystallization due to the absence of phase transformations such as those that occur during cooling of iron or titanium. Recrystallization in aluminum may occur either by continuous or by discontinuous reactions, which exhibit distinct textures and grain boundary characteristics. Selected results from prior work by the authors as well as recent data are combined to illustrate the use of OIM methods in characterizing grain boundaries and their contribution to superplastic deformation as well as failure by cavity growth and coalescence.

This paper was presented at the International Symposium on Superplasticity and Superplastic Forming, sponsored by the Manufacturing Critical Sector at the ASM International AeroMat 2004 Conference and Exposition, June 8-9, 2004, in Seattle, WA. The symposium was organized by Daniel G. Sanders, The Boeing Company.

Keiichiro Oh-ishi, John Boydon, and **Terry R. McNelley,** Department of Mechanical Engineering, Naval Postgraduate School, 700 Dyer Rd., Monterey, CA 93943-5146. Contact email: tmcnelley@nps.edu.

1.1 Grain Size

The constitutive behavior of fine-grain superplastic materials can be described in terms of the independent contributions of grain boundary sliding (GBS) and dislocation creep to the total deformation rate, i.e., $\dot{\varepsilon}_{total} = \dot{\varepsilon}_{gbs} + \dot{\varepsilon}_{\perp}$, where $\dot{\varepsilon}_{gbs}$ and $\dot{\varepsilon}_{\perp}$ are the contributions from GBS and dislocation creep, respectively (Ref 1-4). Grain boundary sliding and its accommodation occur in the boundary and in nearby, mantlelike regions of the grains, so $\dot{\varepsilon}_{gbs}$ is strongly grain size dependent. Dislocation creep occurs in the grain cores, and therefore $\dot{\varepsilon}_{\perp}$ is independent of grain size. Sherby et al. (Ref 3, 4) have combined empirically derived constitutive equations for $\dot{\varepsilon}_{gbs}$ and $\dot{\varepsilon}_{\perp}$ to give:

$$\dot{\varepsilon}_{total} = AD^{*}_{eff}\left(\frac{1}{d}\right)^{2}\left(\frac{\sigma}{E}\right)^{2} + KD\left(\frac{\sigma}{E}\right)^{n} \quad \text{(Eq 1)}$$

where A is a material constant for grain boundary sliding, D^{*}_{eff} is a modified effective diffusion coefficient, d is the grain size, σ is the applied stress, E is Young's modulus, K is a material constant, and D and n are the appropriate diffusion coefficient and stress exponent (3-5) for the dislocation creep mechanism.

Equation 1 predicts a grain-size-dependent transition from dislocation creep at high values of stress and strain rate to superplastic deformation by slip- or diffusion-accommodated grain boundary sliding at lower values of stress and strain rate. This is illustrated in Fig. 1 for a hypothetical material having $D^{*}_{eff} = D$ (the lattice diffusivity) and $n = 5$ (i.e., dislocation climb-controlled creep) by plots of $\dot{\varepsilon}$/D versus σ/E. The transition from dislocation creep to superplasticity is reflected in the change in stress exponent, n ($n \equiv d \log \sigma / d \log \dot{\varepsilon}$), from $n \approx 5$ to $n \approx 2$, which is apparent in Fig. 1. Thus, the strain rate sensitivity coefficient m ($m \equiv 1/n$), increases from ~0.2 to ~0.5, and the latter value is usually sufficient to support the large, neck-free elongations of superplasticity (Ref 1, 3). Clearly, a

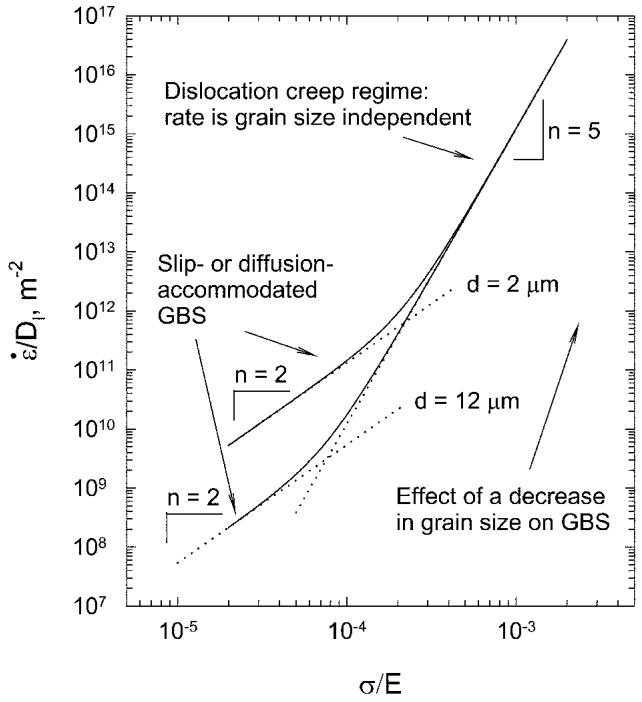

Fig. 1 Diffusion compensated strain rate versus modulus compensated stress for two values of grain size in Eq 1

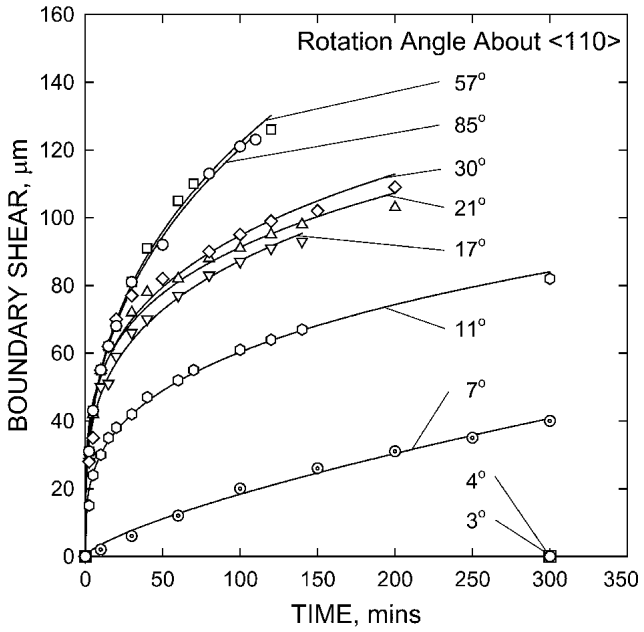

Fig. 2 Boundary shear versus time for GBS at 600 °C in Al tricrystals; replotted from Weinberg (Ref 5)

finer grain size extends upward the range of strain rates for superplasticity, and this is the basis for the requirement that $d \leq 10$ μm for useful superplastic response (Ref 4).

1.2 Grain Boundaries

The lattice registry across boundaries that consist of dislocation arrays precludes sliding of such boundaries, so fine subgrain structures do not support superplasticity. Thus, high-angle boundaries are deemed necessary for the phenomenon. The terms "low-angle" and "high-angle" represent only a partial description of the grain boundary in terms of a lattice orientation relationship, and there have been few detailed investigations of the role of such relationships in GBS. The most recent results are those of Weinberg (Ref 5) 45 years ago (Fig. 2) for boundary pairs in aluminum tricrystals. The data in Fig. 2 apply to the sliding behavior of boundaries having the same grain boundary disorientation angle. A probability distribution rather than such discrete values must be used to represent grain boundary angles in a polycrystal and the dependence of GBS on the distribution of grain boundary disorientation angles has not been determined. Data for Al-Mg-Zr (Ref 6) and Al-Cu-Zr (Ref 7) alloys suggest that the distribution of coincident site lattice (Ref 8) boundaries is not important in superplastic deformation of these alloys. A complete description of a grain boundary in a single-phase polycrystalline material requires the specification of the orientation of the boundary plane as well as the lattice orientation relationship across the boundary. However, serial sectioning is typically required to determine boundary plane orientations.

Randle (Ref 9) has described recently developed OIM methods and their application to the study of grain boundaries. Lattice orientations and grain-to-grain disorientations are readily determined from OIM data. The convention is to define the disorientation as the minimum angle among all crystallographically equivalent rotations that bring grain lattices into coincidence. This angle may be determined by performing a minimization operation among all of the equivalent rotation matrices, that is:

$$\theta_{i,j} \equiv \min \left| \cos^{-1} \left(\frac{(\delta_{11}^{i,j} + \delta_{22}^{i,j} + \delta_{33}^{i,j} - 1)}{2} \right) \right| \quad \text{(Eq 2)}$$

where $\theta_{i,j}$ is the disorientation and the $\delta_{kk}^{i,j}$ are the trace elements of the rotation matrix giving the minimum absolute value of rotation angle. Accordingly, disorientation values are limited to 0-62.8° for cubic materials. The term "correlated disorientation" refers to the disorientations of adjacent grains sharing a common boundary, while "uncorrelated disorientation" is used when the grains do not share a boundary. Only correlated disorientations are examined here, although the uncorrelated disorientation distributions may differ significantly. The latter may be derived from texture data (Ref 10). Randle (Ref 9) discusses a variety of other data representations.

2. Production of Fine Grains and High-Angle Grain Boundaries in Aluminum

2.1 Deformation and Recrystallization

Doherty (Ref 11) has recently reviewed the kinetic theory of nucleation during phase transformations as it applies to recrystallization. During deformation, strain energy is stored in deformation-induced structures comprising mainly dislocations,

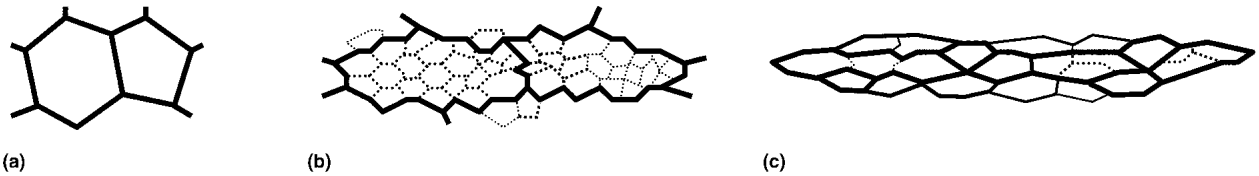

Fig. 3 Schematic illustration of geometric dynamic recrystallization. (a) The original grains. (b) Grain elongation with equiaxed subgrain formation. (c) Pinching off of new grains

and this stored energy is then available for release by recovery (dislocation rearrangement), recrystallization (formation and migration of high-angle grain boundaries), or grain growth (Ref 12). From the standard model for nucleation and growth, the energy barrier (ΔG^*) between the deformed and recrystallized material may be calculated assuming the stored strain energy is given by ρGb^2. For typical dislocation densities and high-angle grain boundary energies, ΔG^* is so large, on the order of 10^5 kT, that the nucleation rate $r \propto \exp(-\Delta G^*/kT)$, must be $\equiv 0$ at any plausible temperature.

In practice, new grains form at finite rates, but they do not form by atom-by-atom coalescence as envisioned in the standard model. Instead, they grow from pre-existing nuclei in the form of small cells or subgrains formed during prior deformation and distributed throughout the deformation microstructure. This accounts for the observation that the orientations of new, recrystallized grains evolve from orientations already present in the deformed state. A complete model of recrystallization requires detailed understanding of deformation-induced microstructures, and investigations (Ref 13) over the past decade have begun to clarify important details of such microstructures. However, predictive models, including the role of alloy constitution, remain to be established.

2.2 Deformation-Induced Microstructures in Aluminum

Deformation processing of aluminum alloys can be carried out by many processes and over a wide range of temperatures and deformation rates. The high stacking fault energy of aluminum results in a predominance of recovery in microstructure evolution. During small-strain tensile creep deformation, the predominant effect of recovery is the formation of subgrains as the prior grains elongate. Fiber texture formation reflects Taylor's criterion for a minimum of five independent slip systems for compatible grain deformation, although GBS at low stresses and sufficient temperatures may relax the slip system requirement (Ref 14).

Deformation processing under hot or warm working conditions involves much larger strains than normally encountered in creep. During rolling, the original grains elongate and become lamellar or ribbonlike in shape, and the area of high-angle grain boundaries greatly increases. In aluminum, grains initially having the cube orientation tend to be stable against lattice rotation and form lamellar bands. The evolving grain shape may also relax the constraints on the number of slip systems required for compatible deformation. Humphreys et al. (Ref 15) has recently shown that geometric dynamic recrystallization (GDRX) during hot or warm working may provide useful grain refinement in rolled aluminum alloys. Equiaxed subgrains form within elongating prior grains and are of a size proportional to $1/Z$, where $Z = \dot{\varepsilon} \exp(Q/RT)$. Z is the Zener-Hollomon parameter. Eventually, the subgrain boundaries interact with high-angle boundaries, which become serrated; this process of grain refinement is illustrated in Fig. 3. As the strain increases and the original grains become thinner, there will be fewer and fewer subgrains across each grain until capillarity effects result in a pinching off of small, equiaxed grains and a recrystallized state, despite the absence of an apparent nucleation event. Geometric dynamic recrystallization (GDRX) takes place gradually and uniformly throughout the microstructure as a continuous recrystallization reaction, and the grain boundaries in the fine-grained, recrystallized state arise from the prior boundaries.

On the other hand, during cold working of aluminum, the original grains elongate and become subdivided by various features. Recent overviews of the processes of grain subdivision have included catalogs of these features, which include lamellar boundaries (LBs), microbands (MBs), and dense dislocation walls (DDWs), as well as subgrains and cellular dislocation structures (Ref 13, 16). The subgrains and cells tend to be equiaxed and to have relatively low angle boundaries. The LBs, MBs, and DDWs are elongated and of larger disorientation and tend to separate regions within original grains that have experienced lattice rotation in opposite senses away from the original grain orientation. The progressive evolution of the deformation microstructure during cold working is illustrated in Fig. 4. The elongation and subdivision of the original grains is shown in Fig. 4(a) to (c); at sufficiently large strains, the prior boundaries are often no longer distinguishable and the microstructure consists of elongated, ribbonlike bands and subgrains, as indicated in Fig. 4(d). Second-phase particles tend to disrupt the bands, and highly refined cell structures form within the deformation zones that develop around the particles, as suggested in Fig. 4(e).

Deformation banding (DB) is also a process of grain subdivision wherein the lattice rotates in different senses in adjacent regions of the grains but toward end orientations in the texture that may be symmetrically related. Deformation banding may start at the initiation of, and continue throughout, deformation, and the bands may become lamellar or ribbonlike in shape at large strains. Equiaxed cells and subgrains develop within the bands as an accommodation mechanism. Barrett and Levenson (Ref 17) suggested the existence of DB in aluminum as early as 1940, although its role in the evolution of deformation-induced microstructures has only recently been recognized (Ref 18).

Deformation banding is prominent in the development of deformation-induced microstructures in rolled superplastic aluminum alloys. Figures 5(a) and (b) provide evidence for DB in the form of OIM grain maps and discrete pole figures for

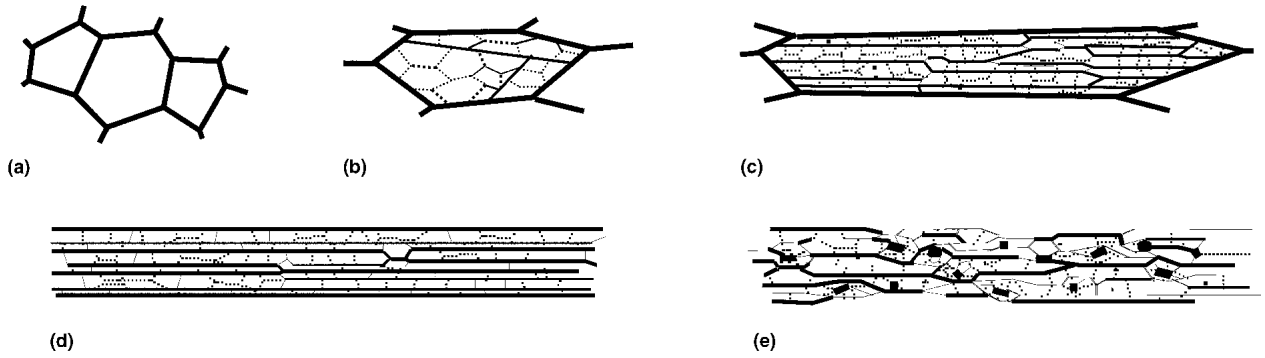

Fig. 4 Schematic representation of the evolution of the deformation microstructure during cold rolling. (a) The original grains. (b) The onset of grain subdivision and substructure formation at small strains. (c) Grain elongation and alignment of high-angle boundaries. (d) The formation of elongated, band-like grains at large strains. (e) The presence of particles disrupts the bandlike structure and leads to formation of deformation zones around the particles.

AA2004 that has been finished by cold rolling. The discrete pole figures illustrate a brass, or B-type, rolling texture component ({011}⟨112⟩, {plane parallel to the rolling plane}⟨direction parallel to the rolling direction⟩) in as-rolled material. Orientation determination by electron backscatter diffraction (EBSD) allows the two distinct variants of the B-texture, which are (110)[11$\bar{2}$] and (011)[21$\bar{1}$], to be separately distinguished by highlighting both the pole figures and the grain maps. Highlighting in either light or dark gray, respectively, of all orientations that lie within 15° of either variant accomplishes this. OIM data include the location of each orientation in the microstructure so that the highlighting will also give the spatial distribution of the orientations in the microstructure as well as in the pole figure. Altogether, these data show that the microstructure is composed of elongated, band-like regions about 2.5 μm in thickness along the thickness direction (ND) and aligned with the rolling direction (RD). In some locations, the bands are immediately adjacent to one another, and at the spatial resolution of OIM (0.2 μm), the interfaces between the bands are high-angle boundaries. The boundary disorientations (50-62.8°, with rotation axes near 111 along the 110-111 symmetry boundary in the unit triangle) correspond closely to the orientation relationship between the variants of the B texture component (60° about the ⟨111⟩ common to both variants). Elsewhere in the image there appear to be transition regions between the bands. Corresponding results are shown in Fig. 5(c) and (d) for cold-rolled AA5083 material, which exhibits a distinct B-type texture and bands varying in thickness from 4 to 8 μm that are aligned with the rolling direction.

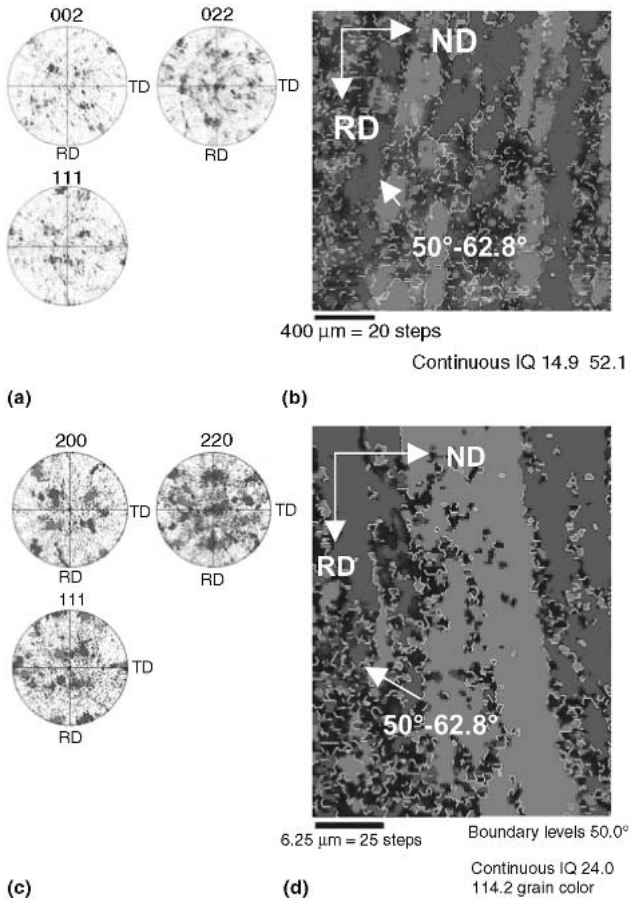

Fig. 5 Discrete pole figures (a) and a grain map for as-rolled Supral 2004, showing alternating bands of the B-texture component (b); as-rolled AA5083 exhibits the same B-texture component (c) and DB structure (d)

2.3 Continuous and Discontinuous Recrystallization in Aluminum

There are two distinct routes for the transformation of cold-rolled microstructures to a superplastic state. The term "continuous recrystallization" has been used to describe stable, homogeneous coarsening of the deformation microstructure (Ref 19). Stable coarsening is favored in cellular structures if, on average, the cells are uniform in size, the boundary mobility is low, there is a narrow spread in boundary mobility, the boundaries are of high disorientation, and there is a narrow range of boundary disorientation. While a uniform cell size within deformation bands will contribute to stable coarsening, the disorientation distribution comprises both low disorientation boundaries (the cell boundaries) and high disorientation boundaries (the interfaces between the deformation bands).

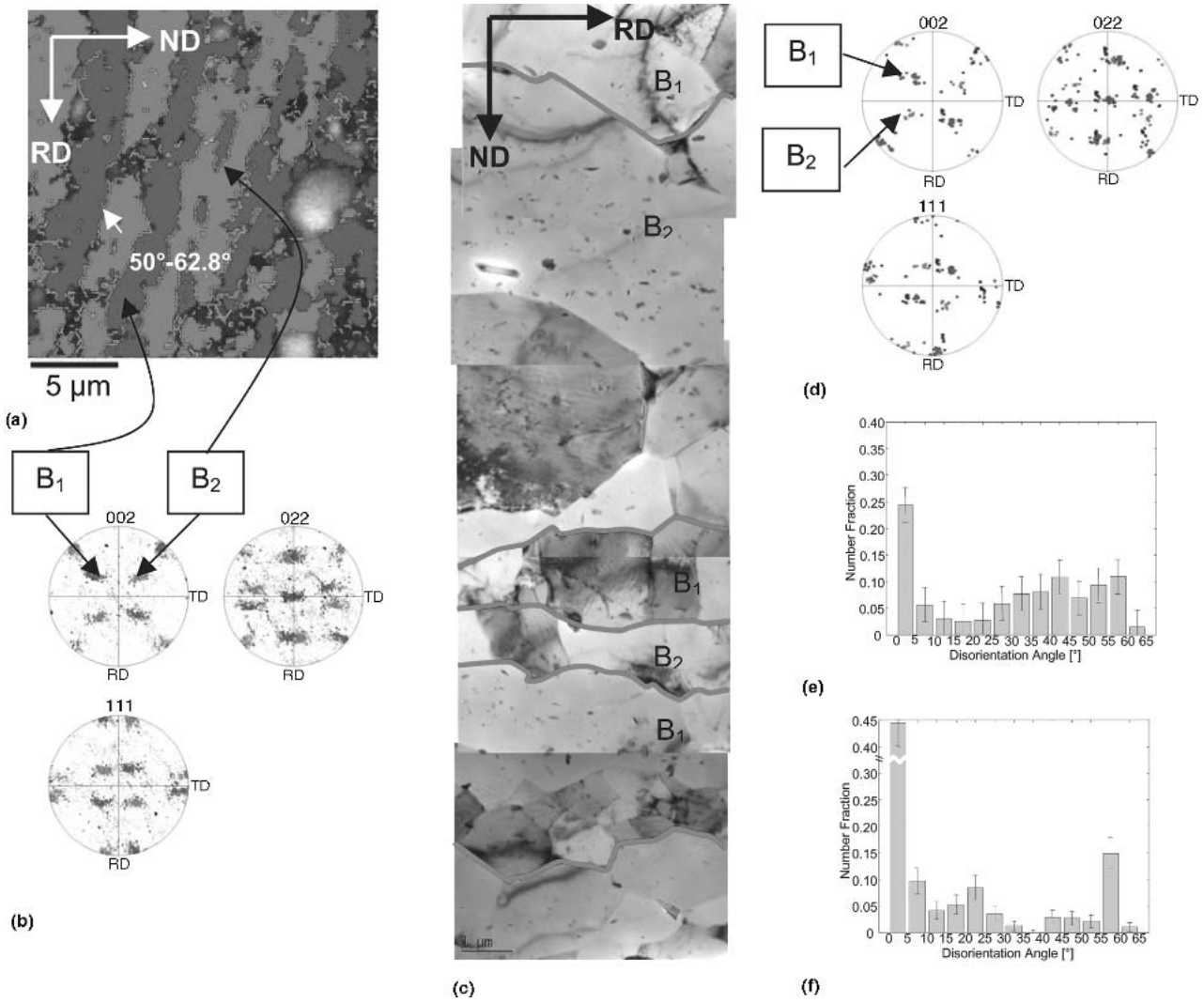

Fig. 6 Microstructural analysis of Supral 2004 annealed at 450 °C showing sharpening of the DB structure in (a) accompanied by sharpening of the B-texture (b); interfaces between the bands are sharp boundaries in TEM (c), while CBED data plotted as pole figures, (d), illustrate the B component as well. The disorientation distributions from (e) OIM and (f) CBED correspond except for the 0-5° range.

Apparently, the presence of a fine, uniform dispersion of Al_3Zr particles, ~30 nm in size, in Al-Cu-Zr alloys such as Supral 2004 suppresses boundary mobility sufficiently for homogeneous coarsening to predominate (Ref 20). In contrast, the term "discontinuous (or primary) recrystallization" is then used to describe unstable coarsening in the deformation microstructure by the long-range migration of mobile boundaries of isolated cells that are highly disoriented with their nearest neighbors. This may appear as a nucleation and growth process in that it involves apparently extensive structural changes that are initially localized spatially and have distinct interfaces between old and new structures. Particle-stimulated nucleation (PSN) of recrystallization in Al-Zn-Mg-Cu and Al-Mg-Mn alloys (Ref 21) and abnormal grain growth are reactions of this type, although the recrystallization "nuclei" were developed during prior plastic deformation and not by thermal fluctuation. Highly mobile boundaries may lead to excessive grain growth that will suppress superplastic response and formability.

2.4 Continuous Recrystallization

Stable coarsening is illustrated in Fig. 6(a) and (b) in the form of OIM grain maps and discrete pole figures for Supral 2004 that has been annealed at 450 °C (this is the superplastic forming temperature for this material). The B-type texture sharpens during this annealing treatment while the bands become more sharply defined. The interfaces between the bands are high angle in nature. A distinct substructure, involving boundaries of 2 to 15° disorientation angle, is present within the bands (Ref 22, 23).

Analysis of this microstructure utilizing convergent beam electron diffraction (CBED) in transmission electron microscopy (TEM) is shown in Fig. 6(c) and (d). In Fig. 6(c), the boundaries appear distinct. High-angle boundaries separate elongated, bandlike regions having orientations corresponding to the symmetric variants of the B texture while a substructure composed of boundaries of lower disorientation is present

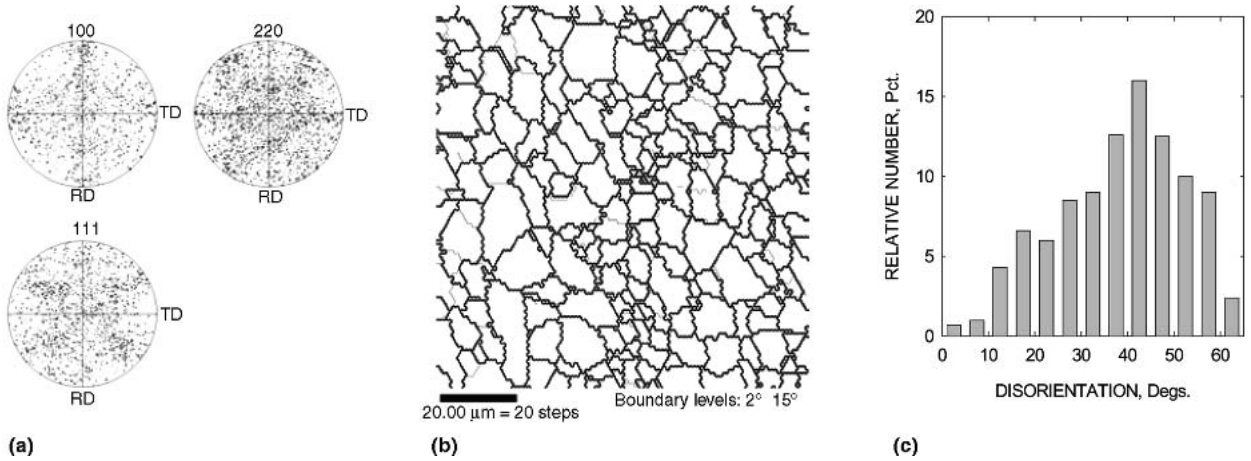

(a) (b) (c)

Fig. 7 (a) Discrete pole figures illustrate a random recrystallization texture due to particle-stimulated nucleation of recrystallization during annealing of AA5083 at 450 °C. (b) The grains are equiaxed and (c) accompanied by a random distribution of grain-to-grain disorientation angles.

within the bands. The B texture is apparent in the pole figures for the TEM data (Fig. 6d), and the spread in lattice orientations suggests moderate disorientations within the substructure. Figures 6(e) and (f) show histograms of disorientation angle distributions based on TEM (Fig. 6e) and OIM (Fig. 6f) analysis; within the standard error these data agree reasonably well (except for 0-5°, due to the finer limit of resolution in OIM) and show that 40 to 60% of the boundaries have disorientation $\geq$15°.

2.5 Discontinuous Recrystallization

Grain refinement for superplasticity in engineering alloys such as AA7475 was achieved via PSN of recrystallization (Ref 21). Overaging treatments are used to develop coarse precipitate particles, ~1 μm in size, prior to cold working. Deformation zones form around the precipitate particles during the cold working and fine, highly disoriented cells evolve within such zones. Humphreys (Ref 24) has derived the conditions for the formation of stable grain nuclei in the deformation zones of sufficiently large particles and, thus, for PSN of recrystallization. Resulting grain sizes tend to be on the order of the spacing of the coarse precipitates, and random textures are characteristic of PSN due to random lattice reorientation in deformation zones during prior straining. OIM data for AA5083 are shown in Fig. 7. The pole figures in Fig. 7(a) illustrate the formation of a random recrystallization texture from the B-type deformation texture of the cold-rolled condition (Fig. 5). Refined equiaxed grains ~12 μm in size, formed by PSN of recrystallization during annealing at 450 °C, are shown in Fig. 7(b), while the histogram in Fig. 7(c) illustrates a random disorientation angle distribution for this material.

3. Deformation and Failure Mechanisms in Superplastic Aluminum Alloys

3.1 Continuous Recrystallization

Mechanical property data in the form of flow stress as a function of strain rate and temperature for the Supral 2004 material are shown in Fig. 8(a). The plots for individual temperatures exhibit a continuous variation in the strain rate sensitivity coefficient (m), which exhibits a maximum value of ~0.5 at a strain rate of 2×10^{-2} s^{-1} at $T = 450$ °C. The corresponding elongation to failure was >800%. Accordingly, a sample of this material was examined by OIM after deformation at this strain rate and temperature to 110% elongation, and the results are summarized in Fig. 8(b) and (c). These data clearly show that the DB structure has persisted and the B texture component has been retained, although the texture has become considerably more diffuse when compared with the annealed condition (Fig. 6). This sample experienced about 45 min at temperature, while the material of Fig. 6 had experienced 6 h at temperature. Thus, strain-enhanced grain growth has resulted in a thickening of the bands with a mean linear intercept grain size of ~5 μm at this deformation strain.

The OIM results for the Supral 2004 material (Fig. 6 and 8) have been interpreted in terms of the DB model (Ref 6, 7). The retention and sharpening of the texture during annealing as well as the appearance of a fine-grain structure in the absence of high-angle boundary migration are consistent with the continuous recrystallization reaction. Thus, the high-angle boundaries that support superplastic deformation in this material have their origins in the interfaces between these bands (Ref 22, 23).

3.2 Discontinuous Recrystallization

Mechanical property and OIM data are provided in Fig. 9 for AA5083 material that has been deformed in uniaxial tension at various strain rates and 450 °C. The strain rate is plotted as a function of modulus-compensated stress in Fig. 9(a). These data illustrate a transition in the deformation mechanism, which is reflected in the change in stress exponent (n) from ~2 to ~4, as the strain rate increases above ~10^{-3} s^{-1}. Thus, the strain rate sensitivity coefficient, $m \equiv 1/n$, decreases from ~0.5 to ~0.25 through the transition. Results of OIM analysis are shown in Fig. 9(b) for a sample deformed at a strain rate of 3×10^{-2} s^{-1} with its tensile axis aligned with the rolling direction (RD) of the material. The OIM data show that grains elongate in the tensile direction, while a subgrain structure develops within the elongating grains. A distinct fiber texture, having

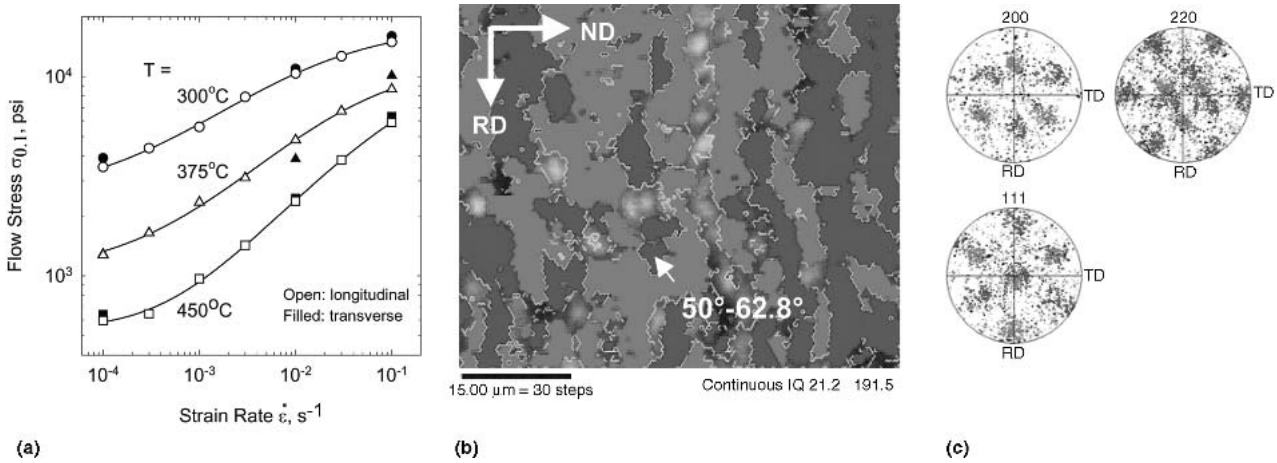

Fig. 8 (a) The flow stress at a strain of 0.1 versus strain rate for elevated-temperature testing of Supral 2004 at of 300, 375, and 450 °C; the maximum strain rate sensitivity coefficient, $m \approx 0.5$, is at 450 °C and 10^{-2} s^{-1} strain rate. (b) The DB structure persists to large strains (110% elongation), and (c) the texture is gradually becoming more diffuse.

both ⟨111⟩ and ⟨001⟩ components, has developed from the random texture of the recrystallized condition (Fig. 7); this is apparent in the pole figures for the deformed material. The grain boundary disorientation distribution exhibits a distinct peak at 0 to 5°, corresponding to subgrain formation during deformation, and a peak at about 40° in the high-angle regime. Results of a corresponding analysis are shown in Fig. 9(c) for a tension test at a strain rate of 3×10^{-4} s^{-1}, which is within the transition region. Grains have coarsened significantly and become somewhat elongated in the tensile direction while fewer subgrain boundaries are evident. Especially noteworthy is the predominance of a random component in the texture as reflected in the absence of preferred orientations in the pole figure data. The grain boundary disorientation distribution is similar to Mackenzie's distribution (Ref 25) for the disorientations of randomly oriented cubes, although a peak at 0-5°, again corresponding to subgrain boundaries, is also apparent. For both deformation conditions of this study, the grain boundary disorientation distributions may be thought of as Mackenzie random distributions with superimposed low-angle peaks.

3.3 Failure by Cavity Growth and Coalescence

The AA5083 material typically exhibited extensive cavity formation during straining under GBS conditions. Despite tensile ductility values >300% elongation, fracture surfaces were often flat and little necking was apparent. Cavities were apparent in OIM images, for example, as shown in Fig. 10(a), although it was necessary to compare corresponding backscatter electron and OIM images to verify that dark regions in OIM gray-scale images were cavities rather than particles not identified in the OIM analysis. The locations in the microstructure as well as local lattice orientations are available in OIM data; thus, grain-to-grain disorientations were evaluated for grains on opposites sides of numerous cavities in a sample deformed to failure at 450 °C in the GBS regime ($\dot{\varepsilon} = 3 \times 10^{-4}$ s^{-1}). This is illustrated in Fig. 10(b), and the resulting data were compiled as histograms, as shown in Fig. 10(c). Comparison of these data to the disorientation distribution for all boundaries in this material, which was presented in Fig. 7(c), reveal that the histograms are similar except that there are no disorientations <7° in the disorientation distribution across the cavities. Despite the presence of a large fraction of low-angle boundaries in the disorientation distribution for all boundaries, as shown earlier in Fig. 4(d), there are, again, no disorientations <7°, suggesting a boundary disorientation threshold for cavity formation.

A threshold value of ~7° is consistent with studies of GBS in aluminum tricrystals (Fig. 2) (Ref 5). Each point in the tricrystal data was obtained for a pair of boundaries that each had the same disorientation. Boundaries of either 3° or 4° disorientation did not slide at $T = 600$ °C, while boundaries having disorientations ≥7° exhibited sliding, and the observed sliding rate increased as disorientation increased. All of the disorientation data in the current study were in the form of distributions and not for isolated boundaries; nevertheless, the absence of low-angle boundaries in the disorientation distributions for cavities is deemed consistent with cavity formation following GBS. Intragranular plastic deformation by dislocation creep and vacancy condensation processes apparently does not contribute appreciably to cavity formation in this material.

4. Summary

Continuous recrystallization involves the development of refined grains with high-angle boundaries in the absence of long-range high-angle boundary migration. Results of OIM analysis have shown that grain subdivision processes, including DB, result in the formation of highly disoriented dislocation boundaries in the deformation microstructure. Continuous recrystallization during static annealing then consists of the recovery-controlled formation of disordered grain boundaries from highly disoriented dislocation boundaries, or transition regions, between bands and between the cells within the bands. Pérez-Prado et al. (Ref 26) have contrasted this perspective to previous models. At the initiation of elevated temperature deformation of such a structure, straining may take place with contributions from both dislocation creep and GBS until high-

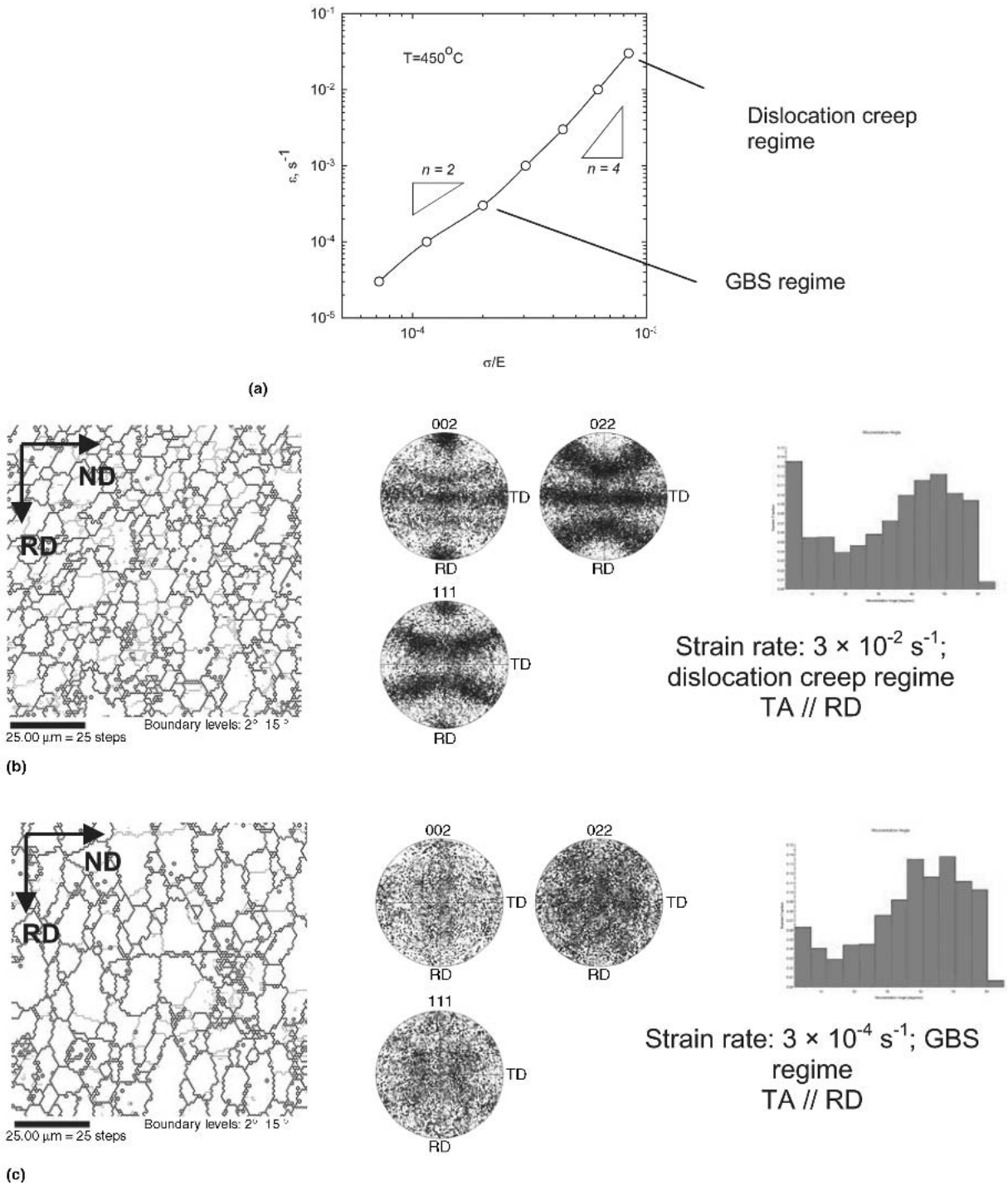

Fig. 9 Mechanical property and OIM data for AA5083 deformed at $T = 450$ °C. (a) Strain rate as a function of modulus-compensated stress, showing dislocation creep and GBS regimes. (b) Grain elongation, substructure formation and fiber texture development in the dislocation creep regime. (c) Grain coarsening, randomizing of texture due to GBS.

angle grain boundaries are fully formed and GBS predominates.

Discontinuous recrystallization associated with PSN at coarse precipitate particles leads to the development of fine, equiaxed grain structures, random textures, and random grain disorientation angle distributions. These features are readily observed using OIM methods. Models for PSN consider the particle dispersion to be dilute and the particles of uniform size. The roles of alloy constitution and the particle size distribution as well as the mechanisms of formation within particle deformation zones of new grain embryos having high-angle boundaries capable of migrating remain to be clarified. Microtexture

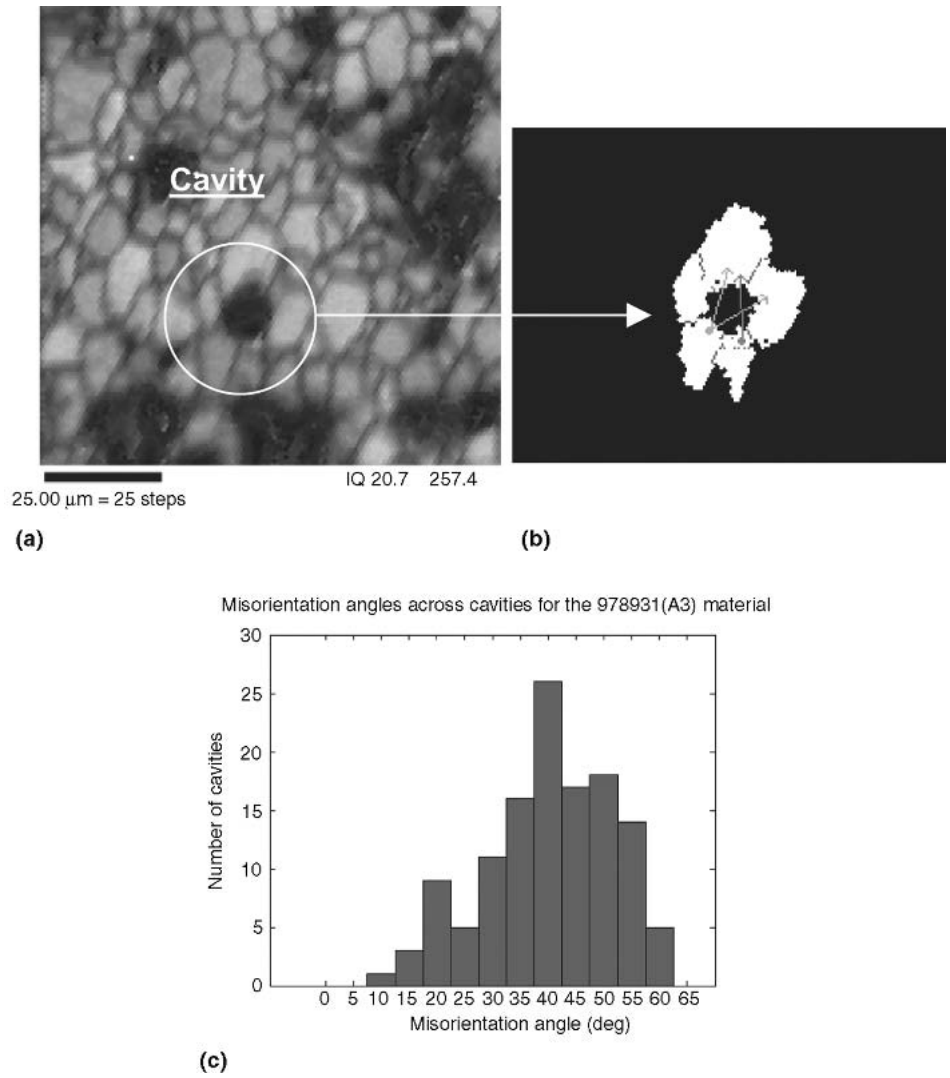

Fig. 10 Determination of disorientations associated with cavities in AA5083. (a) OIM gray-scale image of a cavity. (b) Procedure for determination of disorientations across cavities. (c) Disorientation distributions for cavities in AA5083 material deformed in the GBS regime at $T = 450$ °C and 3×10^{-4} s^{-1} strain rate

and OIM analysis methods may be used to discern regions of transition from dislocation creep to GBS in components, and this may aid in verification of models of the superplastic forming process. Finally, OIM analysis may aid in clarifying mechanisms of cavity formation and growth, leading to failure during forming of components.

References

1. O.D. Sherby and O.A. Ruano, Synthesis and Characteristics of Superplastic Alloys, in *Superplastic Forming of Structural Alloys,* N.E. Paton and C.H. Hamilton, Ed., TMS, 1982, p 241
2. T.G. Langdon, The Mechanical Properties of Superplastic Materials, *Metall. Trans. A,* Vol 13A, 1982, p 689-701
3. O.D. Sherby and J. Wadsworth, Development and Characterization of Fine-Grain Superplastic Materials, in *Deformation Processing and Microstructure,* G. Krauss, Ed., ASM International, 1984, p 355-387
4. O.A. Ruano and O.D. Sherby, On Constitutive Equations for Various Diffusion-Controlled Creep Mechanisms, *Rev. Phys. Appl.,* Vol 23, 1988, p 625
5. F. Weinberg, Grain Boundary Shear in Aluminum, *Trans. Metall. Soc. AIME,* Vol 212, 1958, p 808-817
6. T.R. McNelley and M.E. McMahon, An Investigation by Interactive Electron Backscatter Pattern Analysis of Processing and Superplasticity in an Aluminum-Magnesium Alloy, *Metall. and Mater. Trans. A,* Vol 27A, 1996, p 2252-2262
7. T.R. McNelley and M.E. McMahon, Microtexture and Grain Boundary Evolution During Microstructural Refinement Processes in SUPRAL 2004, *Metall. Mater. Trans. A,* Vol 28A, 1997, p 1879-1887
8. D.G. Brandon, The Structure of High-Angle Grain Boundaries, *Acta Metall.,* Vol 14, 1966, p 1479-1484
9. V. Randle and O. Engler, *Intro. Texture Analysis: Macrotexture, Microtexture and Orientation Mapping,* Gordon and Breach, Amsterdam, 2000
10. B.L. Adams, Description of the Intercrystalline Structure Distribution in Polycrystalline Materials, *Metall. Trans.,* Vol A17, 1986, p 2199-2207
11. R.D. Doherty, D.A. Hughes, F.J. Humphreys, J.J. Jonas, D.J. Jensen, M.E. Kassner, W.E. King, T.R. McNelley, H.J. McQueen and A.D. Rollett, Current Issues in Recrystallization: A Review, *Mater. Sci. Eng. A,* Vol A238, 1997, p 219-274

12. R.D. Doherty, G. Gottstein, J. Hirsch, W.B. Hutchinson, K. Lücke, E. Nes, and P.J. Wilbrandt, Ed., Report of a Panel on Recrystallization Textures: Mechanisms and Experiments, *Proc. ICOTOM 8,* J.S. Kallend and G. Gottstein, Ed., TMS, 1988, p 563
13. D.A. Hughes and N. Hansen, High Angle Boundaries Formed by Grain Subdivision Mechanisms, *Acta Mater.,* Vol 45, 1997, p 3871-3886
14. M.T. Pérez-Prado, G. González-Doncel, O.A. Ruano, and T.R. McNelley, Texture Analysis of the Transition from Slip to Grain Boundary Sliding in a Discontinuously Recrystallized Superplastic Aluminum Alloy, *Acta Mater.,* Vol 49, 2001, p 2259-2268
15. A.Gholinia, F.J. Humphreys, and P.B. Prangnell, Production of Ultra-Fine Grain Microstructures in Al-Mg Alloys by Conventional Rolling, *Acta Mater.,* Vol 50, 2002, p 4461-4476
16. B. Bay, N. Hansen, D.A. Hughes, and D. Kuhlmann-Wilsdorf, Evolution of F.C.C. Deformation Structures in Polyslip, *Acta Metall. Mater.,* Vol 40, 1992, p 205-219
17. C.S. Barrett and L.H. Levenson, The Structure of Aluminum after Compression, *Trans. AIME,* Vol 137, 1940, p 112-127
18. D. Kuhlmann-Wilsdorf, "Regular" Deformation Bands (DBs) and the LEDS Hypothesis, *Acta Mater.,* Vol 47, 1999, p 1697-1712
19. F.J. Humphreys, A Unified Theory of Recovery, Recrystallization and Grain Growth, Based on the Stability and Growth of Cellular Microstructures—I. The Basic Model, *Acta Mater.,* Vol 45, 1997, p 4231-4240
20. B.M. Watts, M.J. Stowell, B.L. Baike, and D. Owen, Superplasticity in Al-Cu-Zr Alloys. I. Material Preparation and Properties, *Metal Sci. J.,* Vol 10, 1976, p 189
21. J.A. Wert, N.E. Paton, C.H. Hamilton, and M.W. Mahoney, Grain Refinement in 7075 Aluminum by Thermo-Mechanical Processing, *Metall. Trans. A,* Vol 12A, 1981, p 1267-1276
22. T.R. McNelley, D.L. Swisher, and M.T. Pérez-Prado, Deformation Bands and the Formation of Grain Boundaries in a Superplastic Aluminum Alloy, *Metall. Mater. Trans. A,* Vol 33A, 2002, p 279-290
23. T.R. McNelley, M.E. McMahon, and M.T. Pérez-Prado, Grain Boundary Evolution and Continuous Recrystallization of a Superplastic Al-Cu-Zr Alloy, *Phil. Trans. R. Soc. Lond. A,* Vol. 357, 1999, p 1683-1705
24. F.J. Humphreys, The Nucleation of Recrystallization at Second Phase Particles in Deformed Aluminum, *Acta Metall.,* Vol 25, 1977, p 1323-1344
25. J.K. Mackenzie, Second Paper on Statistics Associated with the Random Distribution of Cubes, *Biometrika,* Vol 45, 1958, p 229-240
26. M.T. Pérez-Prado, T.R. McNelley, D.L. Swisher, G. González-Doncel, and O.A. Ruano, Texture Analysis of the Transition from Slip to Grain Boundary Sliding in a Continuously Recrystallized Superplastic Aluminum Alloy, *Mater. Sci. Eng A,* Vol A342, 2003, p 216-230